Contribution from Ames Laboratory and the Department of Chemistry, Iowa State University, Ames, Iowa 50011

Characterization, Structure, and Conformations of a Dinuclear Platinum(I) Complex with Mixed Halide–Phosphine Ligands Trans to the Metal–Metal Bond[1]

Reed J. Blau,[†] James H. Espenson,* Sangsoo Kim, and Robert A. Jacobson*

Received August 30, 1985

The X-ray crystal structure of $[Pt_2(\mu\text{-dppm})_2Cl(PPh_3)]^+(PF_6^-)$ indicates considerable tetrahedral distortion of the normally square-planar environment around its PPh_3-ligated platinum. These distortions relieve repulsions between phenyl groups on PPh_3 and those on the adjacent dppm ligand but cause a significant retardation of the rates of axial/equatorial interchange of substituents on the $Pt_2(\mu\text{-dppm})_2$ ring as observed by ^1H NMR spectroscopy. The ^{31}P NMR spectra of this and related complexes are also consistent with these data.

Introduction

The reactivity of the dimeric platinum(I) and palladium(I) complexes with bridging bis(diphenylphosphino)methane (dppm) ligands,[2] such as $Pt_2(\mu\text{-dppm})_2Cl_2$ or, as abbreviated here, (Cl--Cl), has been reviewed elsewhere.[3–5] The conformational fluxionality of related "A"-frame[6] complexes (e.g., $[Pt_2H_2(\mu\text{-H})(\mu\text{-dppm})_2]^+$) and Pt(II) dimers[7] (e.g., *cis*-$[Pt_2Me_4(\mu\text{-dppm})_2]$) has also been treated in considerable detail. Although NMR evidence has been taken to suggest slow conformational fluxionality in Pt(I) dimers, only isolated examples of it have been reported.[8] In other cases, the complexity of the temperature-dependent spectra (e.g., in $(H\text{--dppm})^+$[9] and $(Me\text{--dppm})^+$[10]) hampers their study.

We have found[11] many features common to both the mechanisms of the ligand substitution reactions by which $(Cl\text{--}PPh_3)^+$ is formed from either (Cl--Cl) or $(Ph_3P\text{--}PPh_3)^{2+}$ and those for insertion of small molecules into their respective Pt–Pt bonds.[12,13] We have now characterized the previously unknown complex $(Cl\text{--}PPh_3)^+$ by NMR spectroscopy and X-ray diffraction. The results provide a clear-cut example of Pt(I) dimer fluxionality.

Results and Interpretation

X-ray Crystal Structure. The crystal structure consists of $[Pt_2(\mu\text{-dppm})_2Cl(PPh_3)]^+$ cations, PF_6^- anions, and solvent molecules. The asymmetric unit of the benzene solvate whose structure we determined contains three benzene molecules per ion pair. Three of the fourteen phenyl groups found in the asymmetric unit, including one solvent molecule, are disordered. An ORTEP plot of the ion pair is shown in Figure 1, with one of the orientations of the 1A and 5B groups shown for clarity.

The platinum bound to PPh_3, Pt1, is tetrahedrally distorted (see Figure 2) away from the idealized square-planar geometry. The extent of the distortion is delineated by a comparison of bond angles (Table I) and least-squares planes (Table II) about each platinum. The cis bond angles around Pt1 diverge from 90° in a manner that will accommodate the steric requirements of the bulky PPh_3 group. Some angles are smaller than ideal, e.g., P2–Pt1–P3 (160°) and Pt2–Pt1–P2 (165°), presumably to relieve repulsions between two PPh_3 phenyls, 1B and 1C, and the two adjacent equatorial phenyls of the two respective dppm ligands, 2B and 3A (see Figures 1 and 2). The angles around Pt1 are comparable to those around the Pt to which η^1-dppm is bound in $(H\text{--dppm})^+$.[14]

The $Pt_2P_4C_2$ ring can be regarded as an "extended" cyclohexane ring. In the crystal structure characterized, it exists in a twisted chair conformation (see Figure 2). The least-squares coordination planes of the two metal atoms are rotated about the Pt–Pt bond to intersect at a dihedral angle of 42°. The dihedral angles in $(H\text{--dppm})^+$[14] and (Cl--Cl)[15] are 33.5 and 39°, respectively. Both $[Pt_2(\mu\text{-dppm})(\eta^2\text{-dppm})_2]^{2+}$, with one bridging ligand, and $[Pt_2(CO)_2Cl_4]^{2-}$, with none, have interplanar angles very near 60°.[16] Adoption of a twisted configuration by Pt(I) dimers lowers considerably any antibonding interactions between filled d-π metal orbitals. The dppm methylene carbon C35 deviates by 0.74 Å from the plane defined by P3, P5, and the center of the Pt–Pt bond.

Table I. Selected Interatomic Angles (deg) with Esd's[a] for $[Pt_2(\mu\text{-dppm})_2Cl(PPh_3)](PF_6)\cdot 3C_6H_6$

Pt2–Pt1–P1	164.7 (2)	Pt2–Pt1–P2	82.5 (2)
Pt2–Pt1–P3	84.9 (2)	Pt1–Pt2–Cl	173.3 (3)
Pt1–Pt2–P4	87.3 (2)	Pt1–Pt2–P5	92.7 (3)
P1–Pt1–P2	97.3 (3)	P1–Pt1–P3	160.0 (3)
P2–Pt1–P3	160.0 (3)	Cl–Pt2–P4	88.3 (4)
Cl–Pt2–P5	92.7 (3)	P4–Pt2–P5	176.9 (4)
P2–C24–P4	106.3 (15)	P3–C35–P5	106.7 (20)
Pt1–Pt2–C24	108.3 (9)	Pt1–P3–C35	105.1 (14)
Pt2–P4–C24	115.8 (11)	Pt2–P5–C35	111.5 (14)
Pt1–P1–C11A	113.1 (15)	C11A–P1–C11B	113.7 (18)
Pt1–P1–C11B	110.8 (10)	C11A–P1–C11C	104.0 (20)
Pt1–P1–C11C	112.4 (14)	C11B–P1–C11C	102.3 (17)
Pt1–P2–C21A	114.3 (10)	Pt1–P2–21B	122.5 (12)
C24–P2–C21A	106.7 (13)	C24–P2–C21B	105.1 (15)
Pt2–P3–C31A	120.1 (13)	Pt2–P3–C31B	121.0 (13)
C35–P3–C31A	100.4 (19)	C35–P3–C31B	107.5 (19)
C31A–P3C31B	100.5 (18)		
Pt2–P4–C41A	113.6 (11)	Pt2–P4–C41B	111.8 (19)
C24–P4–C41A	105.7 (15)	C24–P4–C41B	102.5 (21)
Pt2–P5–C51A	115.5 (14)	Pt2–P5–C51B	123.1 (19)
C35–P5–C51A	102.6 (19)	C35–P5–C51B	92.4 (23)
C51A–P5–C51B	107.7 (23)	C51A–P5–D51B	104.3 (29)
C51B–P5–D51B	24.2 (32)	C35–P5–D51B	116.1 (29)
Pt2–P5–D51B	106.9 (26)		

[a] In this and succeeding tables, numbers in parentheses represent estimated standard deviations in the least significant figure.

Table II. Least-Squares Planes and Atomic Deviations Therefrom[a]

Pt1 Plane[b]

atom	shift/Å	atom	shift/Å
Pt1*	−0.016	Cl	0.915
Pt2*	0.325	P4	1.730
P1*	0.301	P5	−1.166
P2*	−0.312	C24	1.257
P3*	−0.297	C35	−1.674

Pt2 Plane[c]

atom	shift/Å	atom	shift/Å
Pt1*	0.088	P1	0.584
Pt2*	−0.020	P2	−1.631
Cl*	0.098	P3	1.317
P4*	−0.087	C24	−1.019
P5*	−0.079	C35	0.266

[a] Atoms used to calculate the plane are marked with an asterisk. [b] $-0.49676X + 0.75125Y + 0.43457Z - 5.14011 = 0.0$. [c] $-0.06172X + 0.99546Y - 0.07249Z - 6.30433 = 0.0$.

The PCH_2P C24 atom appears to be closer to an "envelope" position, since it is displaced from the plane defined by P2, P4,

[†] Henry Gilman Fellow, Iowa State University, 1983–1984.

(1) Based in part on the Ph.D. Thesis of R.J.B., Iowa State University, 1985.

0020-1669/86/1325-0757$01.50/0

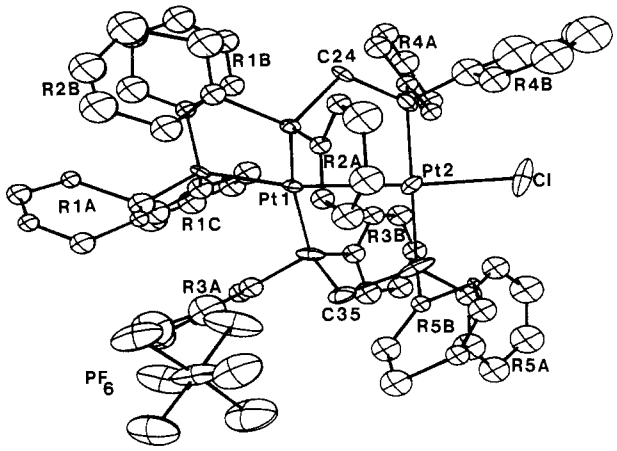

Figure 1. Molecular drawings of $[Pt_2(\mu\text{-dppm})_2Cl(PPh_3)]^+(PF_6)$. Only one of the possible orientations of the disordered 1A and 5B groups is shown for clarity.

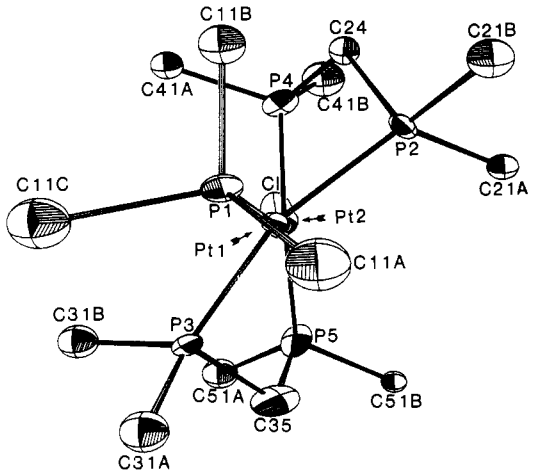

Figure 2. Crystal structure of $[Pt_2(\mu\text{-dppm})_2Cl(PPh_3)]^+$ viewed along the Pt–Pt bond axis. Only the α-carbons of the phenyl groups are shown.

and the center of the Pt–Pt bond by only 0.35 Å.

^{1}H NMR Spectroscopy. Conformational changes of the $Pt_2P_4C_2$ ring of $(Cl\text{--}PPh_3)^+$ are slow on the NMR time scale at ambient temperature. Its ^{1}H NMR spectrum at 20 °C (Figure 3) shows two sets of PCH_2P resonances. One value for $^3J(Pt,H)$ is small, $^3J(Pt,H_{ax}) < 20$ Hz, and the other large, $^3J(Pt,H_{eq}) = 113$ Hz. The H_{eq} resonance consists of three major peaks with area ratios

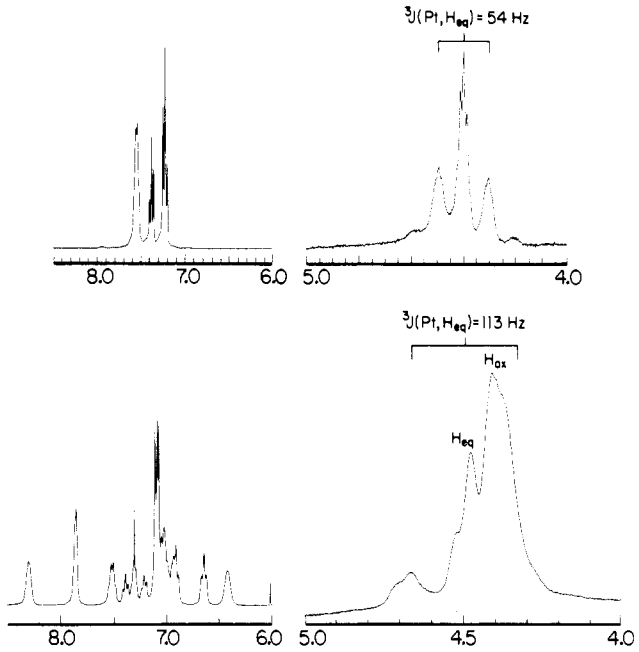

Figure 3. ^{1}H NMR spectra (300 MHz) of $Pt_2(\mu\text{-dppm})_2Cl_2$ (upper) and $[Pt_2(\mu\text{-dppm})_2Cl(PPh_3)](PF_6)$ (lower) at ambient temperature. The left side shows the phenyl region, and the right the PCH_2P region.

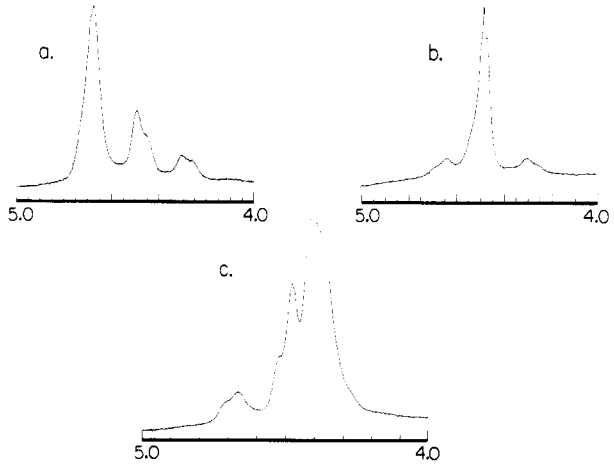

Figure 4. PCH_2P region of the ^{1}H NMR spectra (300 MHz) of $[Pt_2(\mu\text{-dppm})_2Cl(PPh_3)]^+$ with (a) only Cl^- present in CD_2Cl_2, (b) 1.2 Cl^- to 1 PF_6^- in CD_2Cl_2, and (c) only PF_6^- present in $C_2D_2Cl_4$.

1:2.21:1, each split into a doublet by geminal hydrogen coupling with $^2J(H_{eq},H_{ax}) = 13$ Hz. The central doublet in this multiplet is due to the isotopomer of $(Cl\text{--}PPh_3)^+$ containing no ^{195}Pt. The two satellites are due to that containing one ^{195}Pt (i.e., this isotopomer resonance is split into a doublet of doublets).[17] The chemical shift of the unresolved multiplet with $J < 20$ Hz (H_{ax}) is dependent on the counterion present and moves upfield with increasing mole ratio of PF_6^- to Cl^- (see Figure 4).

The assignments of the two resonances were made[18] on the basis of the Karplus[19] correlation, which suggests that the magnitude of vicinal H–H coupling constants is a function of the dihedral angle (θ) between the two hydrogens. This correlation has found general utility for a wide variety of three-bond coupling constants (e.g., $^3J(^{119}Sn,^{13}C)$[20]). Given the dihedral angles between the Pt–P bond and the two types of C–H bonds ($\simeq$70° axial, $\simeq$180°

(2) Puddehphatt, R. J. *Chem. Soc. Rev.* **1983**, *12*, 99.
(3) Balch, A. L. *Adv. Chem. Ser.* **1982**, *No. 196*, 243.
(4) Brown, M. P.; Fisher, J. R.; Franklin, S. J.; Puddephatt, R. J.; Thomson, M. A. *Adv. Chem. Ser.* **1982**, *No. 196*, 231.
(5) (a) Balch, A. L. *ACS Symp. Ser.* **1981**, *No. 155*, 167. (b) Balch, A. L. *Comments Inorg. Chem.* **1984**, *3*, 51.
(6) Puddephatt, R. J.; Azam, K. A.; Hill, R. H.; Brown, M. P.; Nelson, C. D.; Moulding, R. P.; Seddon, K. R.; Grossel, M. C. *J. Am. Chem. Soc.* **1983**, *105*, 5642.
(7) Manojlovic-Muir, Lj.; Muir, K. W.; Frew, A. A.; Ling, S. S. M.; Thomson, M. A.; Puddephatt, R. J. *Organometallics* **1984**, *3*, 1637.
(8) Brown, M. P.; Franklin, S. J.; Puddephatt, R. J.; Thomson, M. A.; Seddon, K. R. *J. Organomet. Chem.* **1979**, *178*, 281.
(9) Brown, M. P.; Fisher, J. R.; Hill, R. H.; Puddephatt, R. J.; Seddon, K. R. *Inorg. Chem.* **1981**, *20*, 3516.
(10) Azam, K. A.; Brown, M. P.; Hill, R. J.; Puddephatt, R. J.; Yavari, A. *Organometallics* **1984**, *3*, 697.
(11) Blau, R. J.; Espenson, J. H. *J. Am. Chem. Soc.*, in press.
(12) Muralidharan, S.; Espenson, J. H. *Inorg. Chem.* **1983**, *22*, 2786.
(13) Muralidharan, S.; Espenson, J. H. *J. Am. Chem. Soc.* **1984**, *106*, 8104.
(14) Manojlovic-Muir, Lj.; Muir, K. W. *J. Organomet. Chem.* **1981**, *219*, 129.
(15) Manojlovic-Muir, Lj.; Muir, K. W.; Solomun, T. *Acta Crystallogr., Sect. B: Struct. Crystallogr. Cryst. Chem.* **1979**, *B35*, 1237.
(16) Al-Resayes, S. I.; Hitchcock, P. B.; Nixon, J. F. *J. Organomet. Chem.* **1984**, *267*, C13.
(17) Brown, M. P.; Puddephatt, R. J.; Rashidi, M.; Seddon, K. R. *J. Chem. Soc., Dalton Trans.* **1977**, 951.
(18) Blau, R. J. Ph.D. Thesis, Iowa State University, 1985.
(19) Karplus, M. *J. Am. Chem. Soc.* **1963**, *85*, 2870.
(20) Doddrell, D.; Burfitt, I.; Kitching, W.; Bullpitt, M.; Lee, C.-H.; Mynott, R. J.; Considine, J. L.; Kuivila, H. G.; Sarma, R. H. *J. Am. Chem. Soc.* **1974**, *96*, 1640 and references therein.

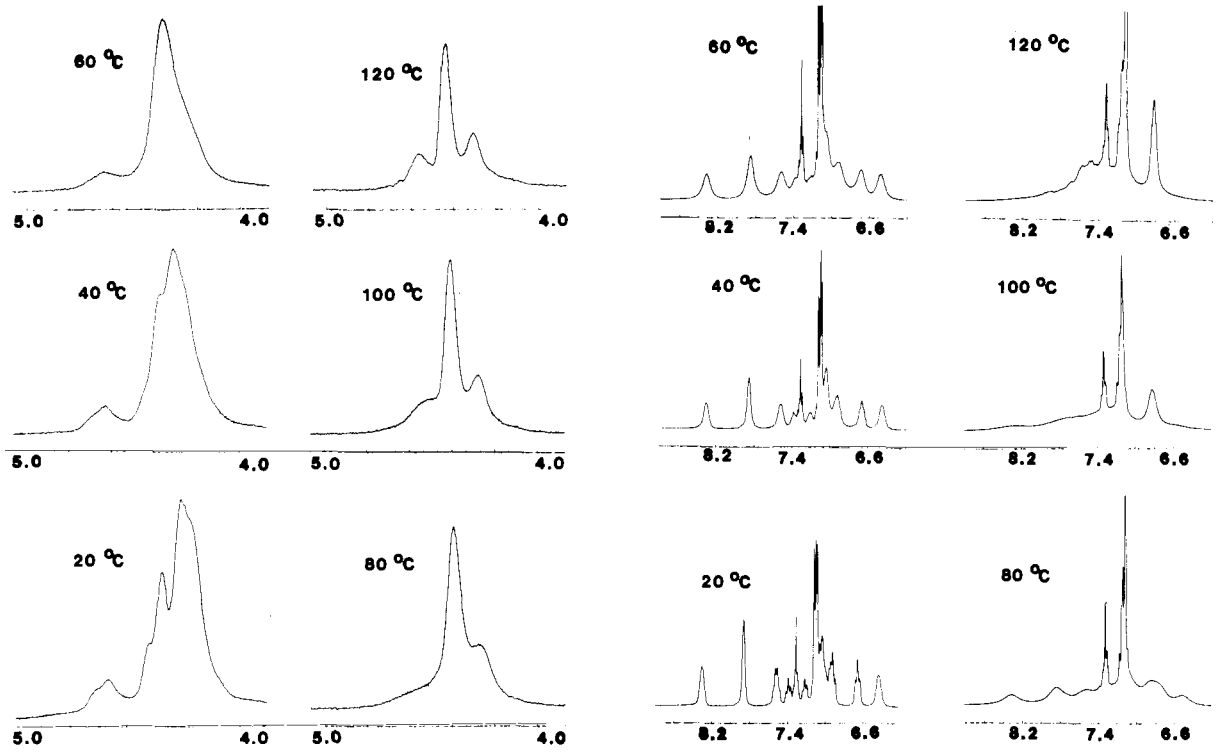

Figure 5. Temperature-dependent ^{1}H NMR spectra (300 MHz) of $[Pt_2(\mu\text{-dppm})_2Cl(PPh_3)]^+$ in $C_2D_2Cl_4$ showing the regions for the PCH_2P (left) and phenyl (right) resonances.

equatorial), we assigned the equatorial protons to the proton resonance with a 113-Hz Pt–H coupling constant. According to this assignment, the H_{ax} resonance undergoes counterion-dependent shifts, (e.g., Figure 4). This is logical since negatively charged counterions will most likely be associated with the Pt centers, and their presence will cause greater perturbations in the chemical shift of axial protons while leaving the shift of equatorial protons largely unaffected.

As the temperature increases, the two PCH_2P resonances coalesce into one 1:2.21:1 triplet with a ^3J(Pt,H) value of 57 Hz, the average of the slow-exchange limit values. Its unsymmetrical structure (see Figure 5) is due to the difference in the coalescence temperatures of the low-field (T_c = 360 ± 10 K) and high-field (T_c = 333 ± 10 K) satellites. Although the majority of the phenyl resonances broaden and coalesce simultaneously with the PCH_2P resonances, two phenyl multiplets remain essentially unchanged throughout the temperature range (see Figure 5). The computer-integrated intensities of the two types of protons gave a broadened:nonbroadened ratio of 2.42 ± 0.13 at three selected temperatures. Apparently, an axial/equatorial exchange process causes interconversion of the environments of both the PCH_2P hydrogens and the dppm phenyl rings, whereas the PPh_3 phenyls are locked into a single, nonexchanging environment. The theoretical ratio of dppm:PPh_3 phenyl hydrogens is 2.67, in good agreement with experiment.

Rate constants at the various coalescence temperatures were evaluated from both the PCH_2P and phenyl regions of the spectrum. All of the values so obtained define a single linear plot of ln (k/T) vs. $1/T$ (Figure 6). Thus, the process that causes signal averaging of both the phenyl and PCH_2P proton resonances is the same since it is characterized by a single set of activation parameters. The value of $\Delta S^\ddagger$ = −0.7 ± 3.4 cal mol^{-1} K^{-1} is essentially zero, which appears very reasonable for a conformational change. The value of $\Delta H^\ddagger$ is 16.5 ± 1.1 kcal/mol, only slightly higher than the upper limit for conformational changes of substituted cyclohexanes.[21]

^{31}P NMR Spectroscopy. The $^{31}P\{^1H\}$ spectrum of $(Cl\text{--}PPh_3)^+$ consists of three complex multiplets with accompanying ^{195}Pt

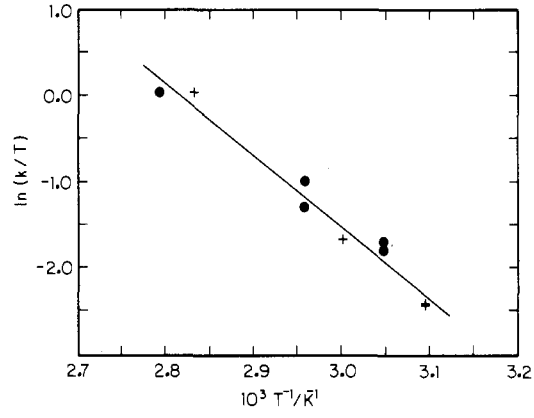

Figure 6. Coalescence temperatures (T) and corresponding experimental rate constants for axial/equatorial exchange (k) from the phenyl (+) and PCH_2P (●) regions of the ^{1}H NMR spectra (300 MHz) of $[Pt_2(\mu\text{-dppm})_2Cl(PPh_3)]^+$ plotted as ln (k/T) vs. $1/T$ to yield $\Delta H^\ddagger$ = 16.5 ± 1.1 kcal/mol and $\Delta S^\ddagger$ = −0.7 ± 3.4 cal mol^{-1} K^{-1} for the exchange process.

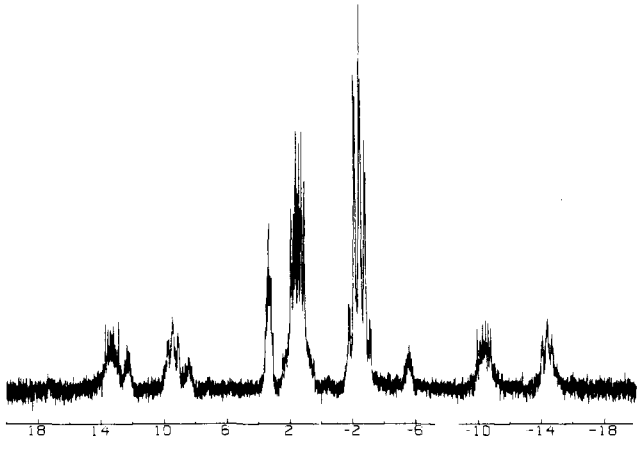

Figure 7. $^{31}P\{^1H\}$ NMR spectrum of $[Pt_2(\mu\text{-dppm})_2Cl(PPh_3)]^+$ in CD_2Cl_2 (P_T = PPh_3).

(21) Kessler, H.; Gusowski, V.; Hancock, M. *Tetrahedron Lett.* **1968**, *9*, 4665.

Table III. ^{31}P NMR Coupling Constants (Hz) for $[Pt_2(\mu\text{-dppm})_2X(PR_3)]^+$ Complexes

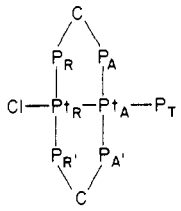

coupling const	$(Cl\text{--}PPh_3)^{+a}$	$(I\text{--}PPh_3)^{+b}$	$(Cl\text{--}dppm)^{+a}$
$^2J(P_A,P_R)$	68.7		
$^3J(P_A,P_R)$	11.0		
$^2J(P_T,P_A)$	19.0	20.7	
$^3J(P_T,P_R)$	8.3	7.3	
$^1J(Pt_A,P_A)$	2876	2857	2921
$^1J(Pt_R,P_R)$	2894	2839	2872
$^1J(Pt_A,P_T)$	2186	2213	2146
$^2J(Pt_R,P_T)$	1232	1258	1270
$^2J(Pt_R,P_A)$	±142		
$^2J(Pt_A,P_R)$	±37		

[a] Additional parameters used in the spectral simulations were δr = 393 Hz, $^2J(P_A,P_{A'})$ = 576.6 Hz, and $^2J(P_R,P_{R'})$ = 500 Hz. [b] P,P coupling patterns were not simulated.

satellites. The approximate peak areas are in a ratio of 1:2:2 (see Figure 7). The same spectrum is observed upon the addition of 1 equiv of Cl^- to $(Ph_3P\text{--}PPh_3)^{2+}$ and upon the addition of 1 equiv of PPh_3 to (Cl--Cl), as in eq 1.

$$(Cl\text{--}Cl) \xrightarrow[-Cl^-]{+PPh_3} (Cl\text{--}PPh_3)^+ \xleftarrow[-PPh_3]{+Cl^-} (Ph_3P\text{--}PPh_3)^{2+} \quad (1)$$

For a discussion of the ^{31}P NMR spectrum, the positions are designated relative to the phosphorus of the terminal triphenylphosphine, P_T, as in I.

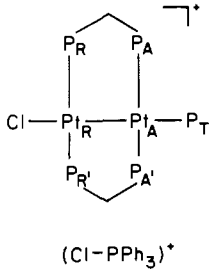

$(Cl\text{-}PPh_3)^+$

The smallest resonance, assigned to the P_T, consists of a 19-Hz triplet split by an 8.3-Hz triplet. The dppm resonances were assigned from the coupling constants $^3J(P_R,P_T)$ = 9 Hz and $^2J(P_A,P_T)$ = 20 Hz (see Table III).

Each of the dppm resonances can be viewed as a half-spectrum of an AA′BB′ system in which each of the theoretical[22] lines is split into either an 8.3-Hz (P_R) or a 19-Hz (P_A) doublet by coupling with P_T. Spectral simulation (see Figure 8) allowed the determination of all other coupling constants and chemical shifts (Table III). Except for $^2J(P_A,P_{A'})$ and $^2J(P_R,P_{R'})$, the values were determined with reasonable precision. The sum (K) and difference (M) between J(A,A′) and J(B,B′) can often be extracted. In this case M = 73.6, but K could not be determined because the least intense outermost lines in each half-spectrum were not observed.

The respective Pt–P coupling constants (Table III) are also consistent with the presence of a strong Pt–Pt bond. A large trans $^2J(Pt_R,P_T)$ of 1232 Hz (Figure 7) is comparable to trans ^2J(Pt,P) in other Pt(I) dimers.[23] However, values of cis $^2J(Pt_R,P_A)$ and cis $^2J(Pt_A,P_R)$ in $(X\text{--}PPh_3)^+$ and analogous values reported for other Pt(I) dimers[24] are consistently less than 150 Hz. This

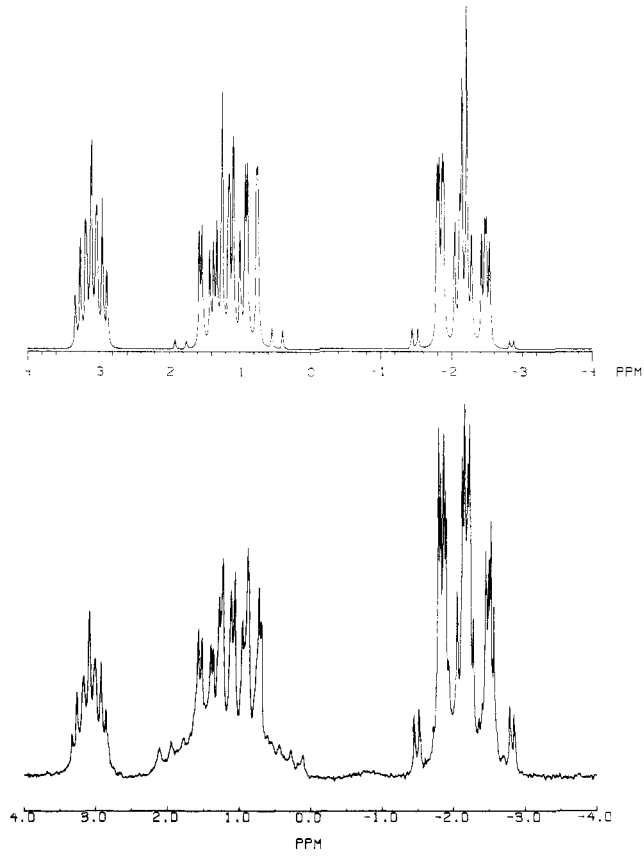

Figure 8. Central resonances (bottom) in the $^{31}P\{^1H\}$ NMR spectrum of $[Pt_2(\mu\text{-dppm})_2Cl(PPh_3)]^+$ in CD_2Cl_2. The spectrum was simulated by using the coupling constants in Table III with $\delta(P_A)$ = 1.12, $\delta(P_R)$ = −2.13, and $\delta(P_T)$ = 3.08.

disparity points to significant orbital overlap between two trans-disposed substituents that is absent when they are cis, because significant overlap can occur only through a metal–metal bond.

The $^1J(Pt_A,P_T)$ value of 2186 Hz is considerably smaller than the $^1J(Pt_A,P_A)$ and $^1J(Pt_R,P_R)$ values of 2876 and 2894 Hz; P_T is trans to a Pt–Pt bond whereas P_A and P_R are trans to a phosphine. Because the Pt–Pt bond exerts a larger trans influence than a phosphine,[9] the Pt–P_T bond is weaker, yielding a smaller coupling constant. In summary, the Pt–P coupling constants observed for $(Cl\text{--}PPh_3)^+$ are consistent with the dppm ligands being cis to a strong Pt–Pt bond and the PR_3 ligand being trans to it.

The patterns of P–P and Pt–P coupling constants in the ^{31}P NMR spectrum of $(I\text{--}PPh_3)^+$ are similar to those found for $(Cl\text{--}PPh_3)^+$ (see Table III). The same is true for $(Cl\text{--}dppm)^+$, which is, however, further complicated by the coupling with the "dangling" phosphorus atom of the η^1-dppm ligand.

Discussion

The eleven phenyl rings in $[Pt_2(\mu\text{-dppm})_2Cl(PPh_3)]^+$, especially the three bound to PPh_3 that compete with the four on the adjacent dppm ligands for vibrational and rotational freedom, cause distortions of the idealized square-planar geometry around each platinum center. Moreover, we believe that it is the necessity to avoid phenyl–phenyl interactions that retards the rates of conformational changes in this molecule.

Distortion around Square-Planar Platinum. It appears that steric repulsions in $(Cl\text{--}PPh_3)^+$ are relieved through distortions of the idealized square-planar environment of Pt1 and not through elongation of the Pt–PPh_3 bond. The latter bond distance of 2.333 Å is by no means out of the ordinary considering the trans influence of the Pt–Pt bond.[23] In $(Ph_3P\text{--}PPh_3)^{2+}$ the Pt–PPh_3 bond

(22) Gunther, H. *Angew. Chem., Int. Ed. Engl.* **1972**, *11*, 861.
(23) Blau, R. J.; Espenson, J. H. *Inorg. Chem.* **1986**, *25*, 878.
(24) Brown, M. P.; Fisher, J. R.; Franklin, S. J.; Puddephatt, R. J.; Seddon, K. R. *J. Organomet. Chem.* **1978**, *161*, C46.
(25) Blau, R. J.; Espenson, J. H., unpublished results.
(26) Brown, M. P.; Fisher, J. R.; Puddephatt, R. J.; Seddon, K. R. *Inorg. Chem.* **1979**, *18*, 2808.

Table IV. ^3J(Pt,H) (Hz) for PCH_2P Hydrogens in Selected $Pt_2(\mu\text{-dppm})_2$ Complexes

complex	nonequiv H's[a] $^3J(Pt,H_{ax})$	$^3J(Pt,H_{eq})$	complex	equiv H's[a] ^3J(Pt,H)
$(Cl\text{--}PPh_3)^+$ [b]	<10	113	$(Cl\text{--}PPh_3)^+$ [c]	57
$(Cl\text{--}dppm)^+$	<10	124	$(H\text{--}PPh_3)^+$ [d]	40, 72
$(Cl\text{--}P_4\text{--}Cl)^{2+}$ [e]	<10	110	$(H\text{--}PMe_2Ph)^+$ [d]	38, 68
$(Cl\text{–}CH_2\text{–}Cl)$ [f]	10	57	$(Cl\text{--}Cl)$ [g]	54
$(Ph_3P\text{–}CH_2\text{–}PPh_3)^{2+}$ [h]	12	48	$(Ph_3P\text{--}PPh_3)^{2+}$ [i]	56

[a] Unless otherwise specified, the NMR solvent is CD_2Cl_2. [b] This spectrum was acquired at 20 °C in $C_2D_2Cl_4$. [c] This spectrum was acquired at 120 °C in $C_2D_2Cl_4$. [d] From ref 9. [e] $[\{Pt_2Cl(\mu\text{-dppm})_2\}_2(di\text{-}\eta^2\text{-}P_4)]^{2+}$.[25] [f] $[Pt_2(\mu\text{-dppm})_2(\mu\text{-}CH_2)Cl_2]$.[26] [g] From ref 17. [h] $[Pt_2(\mu\text{-dppm})_2(\mu\text{-}CH_2)(PPh_3)_2]^{2+}$.[13] [i] From ref 8.

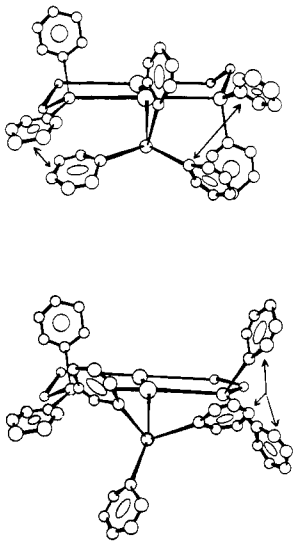

Figure 9. Models for $[Pt_2(\mu\text{-dppm})_2Cl(PPh_3)]^+$ in a chair configuration (top) and a boat/chair transition (bottom). The arrows point from PPh_3 to those on dppm ligands that collide upon rotation of PPh_3 about the Pt–P bond.

distance has been estimated as 2.37 ± 0.02 Å from the relation[23] between Pt–P bond distance and corresponding Pt–P coupling constant. Inward distortion of the $Pt(\mu\text{-dppm})_2$ ring from both directions may not be as favorable in the symmetric complex, leaving the Pt–P bond elongation as the only alternative to relieve steric repulsions.

Axial/Equatorial Exchange. Less steric respulsion between dppm and PPh_3 phenyls exists when the PCH_2P methylenes are in out-of-plane configurations. In either a boat or chair form, rotation about the Pt–PPh_3 bond is hindered only by the two equatorial phenyls bound to the P_A of each bridging dppm (see Figure 9). The angle of rotation (ω_t) of the Pt–PPh_3 bond estimated from "ball and stick" models of the complex in a boat or chair form is about 60°. As a PCH_2P methylene becomes planar, the angle of this Pt–PPh_3 bond rotation is further restricted (ω_t = 25°) by contact of the two dppm phenyls bound to the P_A of the planar PCH_2P group with the PPh_3 phenyl (see Figure 9). Because the constrained PPh_3 phenyl *bisects the angle* between the two dppm phenyls, ω_t can increase from 25 to 55° when the Pt–P bond is increased from 2.2 to 2.4 Å. *We thus infer that the rate of boat/chair isomerization is very sensitive to the Pt–P bond distance.* This hypothesis, although not yet tested in detail, satisfies all known cases.

Proton NMR of Related Complexes. The two ^1H NMR resonances of the dppm methylene protons in $(Cl\text{--}PPh_3)^+$ are inequivalent. In contrast, (Cl--Cl) (see Figure 3), $(Ph_3P\text{--}PPh_3)^{2+}$, and several analogues have CH_2 protons that are equivalent on the ^1H NMR time scale.

Table IV lists values of ^3J(Pt,H) for the PCH_2P hydrogens in a number of $Pt(\mu\text{-dppm})_2$ complexes. The values for Pt(I) complexes containing equivalent PCH_2P hydrogens are the approximate average of the two ^3J(Pt,H)'s in Pt(I) complexes with inequivalent hydrogens (e.g., Figure 3). Inequivalent hydrogens are observed only in those Pt(I) complexes that have a potential for significant phenyl–phenyl repulsion during the axial/equatorial transition. We also note data in the literature that suggest to us that conformational changes of the $Pt_2P_4P_2$ rings in $(H\text{--}dppm)^+$ [9] and $(Me\text{--}dppm)^+$ [10] may also be slow on the ^1H NMR time scale. The ^1H NMR spectrum of $(I\text{--}PPh_3)^+$ and of $(Cl\text{--}dppm)^+$, although less thoroughly investigated, are also indicative of inequivalent PCH_2P hydrogens.

Steric repulsions in $(Ph_3P\text{--}PPh_3)^{2+}$ should be sufficient to lower the rate of its boat/chair isomerization. The PCH_2P protons in this complex are equivalent, however, and in fact, remain so down to −80 °C. This finding cannot be explained by dissociation of the PPh_3 ligand for the following reasons: (1) The sum of the rate constants estimated for PPh_3 dissociation (0.03 s^{-1})[11] and Pt–dppm dissociation, which amounts to Pt_2P_2C ring opening[13] (0.027 s^{-1}), is 1 order of magnitude lower than the value estimated for exchange (0.83 s^{-1}) in $(Cl\text{--}PPh_3)^+$ at 25 °C. (2) The rate constant for axial/equatorial exchange in $(Ph_3P\text{--}PPh_3)^{2+}$ must be *much faster* than 0.83 s^{-1} at 25 °C because the $(Cl\text{--}PPh_3)^+$ resonances are at the slow-exchange limit whereas those of $(Ph_3P\text{--}PPh_3)^{2+}$ are at the fast-exchange limit at this temperature.

We thus look to an explanation that resides in a different phenomenon, namely a lowering of the barrier by Pt–PPh_3 elongation. A long Pt–PPh_3 bond length in $(Ph_3P\text{--}PPh_3)^{2+}$ has already been predicted because of the dissociative nature of its reactions[11,13] and its extraordinarily low value for $^1J(Pt,P_T)$.[23]

Two ^3J(Pt,H) coupling constants have been reported (see Table IV) for $(H\text{--}PMe_2Ph)^+$ and $(H\text{--}PPh_3)^+$ at the fast-exchange limit. This signals the inequivalence of the Pt atoms in these complexes. The same was expected for $(Cl\text{--}PPh_3)^+$, but in this case they were not resolved.

Summary. $(Cl\text{--}PPh_3)^+$, $(I\text{--}PPh_3)^+$, and $(Cl\text{--}dppm)^+$ have sufficient phenyl–phenyl repulsions to cause a significant retardation of the rates of axial/equatorial interchange of substituents on the $Pt_2(\mu\text{-dppm})_2$ ring. On the other hand, such phenyl–phenyl repulsions are insufficient to cause significant elongation of the Pt–PR_3 bond to the point that Pt–Cl bond formation is thermodynamically favored over Pt–phosphine formation (i.e., in $[Cl\text{--}P(o\text{-tol})_3]^+$ and $(Ph_3P\text{--}PPh_3)^{2+}$).[11]

Experimental Procedures

Solvents. Most solvents (dichloromethane, methanol, benzene, chloroform, and acetone) were used as purchased. Dichloromethane-d_2 (99.5% D) was used in obtaining NMR spectra at ambient and low temperatures. The deuterated solvent 1,1,2,2-tetrachloroethane-d_2 (98% D) was used for the same purpose at high temperatures.

Reagents. The salts $[Et_4N]Cl$ and $[Et_4N]PF_6$ were recrystallized from acetone–CH_2Cl_2–hexanes (2:2:1) and methylene chloride–hexanes, respectively. NH_4PF_6 and bis(diphenylphosphino)methane were used as purchased, whereas PPh_3 was recrystallized from either ethanol or methylene chloride–hexanes. $[Pt_2(\mu\text{-dppm})_2Cl_2]$[17] and $[Pt_2(\mu\text{-dppm})_2(PPh_3)_2](PF_6)_2$[8] were synthesized by literature methods.

$[Pt_2(\mu\text{-dppm})_2X(PR_3)]^+$. $(Cl\text{--}PPh_3)^+$ was synthesized by the addition of 0.0488 g (0.170 mmol) of PPh_3 to a 5-mL CH_2Cl_2 solution containing 0.149 g (0.114 mmol) of (Cl--Cl). After 5 min, 0.062 g (0.22 mmol) of $[Et_4N]PF_6$ was added and the resulting crude $[Pt_2(\mu\text{-dppm})_2Cl(PPh_3)](PF_6)$ was precipitated by the addition of pentanes. The complex was purified on a column of Baker 60–200 mesh silica gel. The crude product was eluted by using CH_2Cl_2 until the resulting yellow band was one-half to two-thirds of the way down the column. An acetone–chloroform (9:1) mixture was then used to elute the band in a concentrated form. The bright yellow solid obtained by addition of pentane to this solution contains no $[Et_4N]^+$ salts, as substantiated by ^1H NMR. Its

Table V. Parameters from the Temperature-Dependent ^{1}H NMR (300-MHz) Spectra of $[Pt_2(\mu\text{-dppm})_2X(PPh_3)]^+$

δ_A[a]	δ_B[a]	$\Delta\nu$/Hz[b]	k_{ex}/s^{-1}[c]	T_c/K
7.528	7.507	6.26	27.8	323
6.941	6.919	6.46	28.7	323
4.710	4.655	12.5	55.4	328
4.520	4.478	13.5	59.8	328
6.679	6.632	14.2	63.2	333
4.478	4.408	21.0	93.2	338
4.687	4.500	28.0	124	338
6.929	6.655	81.8	364	353
4.687	4.410	83.1	369	358

[a] Positions of pairs of coalescing peaks at 20 °C. [b] $\Delta\nu = \nu_A{}^0 - \nu_B{}^0$. [c] Calculated by using eq 2.

resonances in the ^{31}P NMR spectrum occur at 1.12 (P_A), −2.13 (P_R), and 3.08 (P_T) ppm.

The complex $(I\text{--}PPh_3)^+$ may be synthesized on a 10–40 mM scale by addition of excess PPh_3 to (I--I) in CH_2Cl_2 or by the addition of a tenfold excess of $[(n\text{-}Bu)_4N]I$ to $(Ph_3P\text{--}PPh_3)^{2+}$ in CH_2Cl_2 followed by allowing the resulting solution to remain at room temperature for at least 2 h. Attempts were not made to isolate this complex as a purified solid, and data were taken in solution. Its ^{31}P NMR spectrum has resonances centered at 6.7 (P_T), 0.1 (P_A), and −6.6 (P_R) ppm.

$(Cl\text{--}dppm)^+$ was synthesized on a 10–40 mM scale by the addition of a slight excess of dppm to (Cl--Cl). It also was not isolated as a purified solid but was characterized by ^{31}P NMR with resonances centered at −2.6 (P_T), 1.0 (P_A), −2.0 (P_R), and −29.5 (uncoordinated P) ppm.

Instrumentation. Routine ^{1}H NMR spectra were recorded by using a Nicolet NT-300 spectrometer in the FT mode, and variable-temperature ^{1}H NMR measurements were obtained by using a Bruker WM 300 spectrometer. The $^{31}P\{^1H\}$ NMR were recorded by using the latter spectrometer operating at 121.5 MHz. Splitting patterns in $^{31}P\{^1H\}$ NMR spectra were simulated by using software (NMC-SIM) provided with the Nicolet NT-300 spectrometer.

Methods. Coalescence temperatures for peaks in the ^{1}H NMR spectra of $(Cl\text{--}PPh_3)^+$ (Figure 5) were estimated via interpolation. Corresponding rate constants (k_{ex}) for the axial–equatorial positional exchange of substituents on the $Pt_2(\mu\text{-dppm})_2$ ring were calculated by using

$$k_{ex} = 2^{1/2}\pi(\nu_A{}^0 - \nu_B{}^0) \quad (2)$$

where $\nu_A{}^0$ and $\nu_B{}^0$ are the frequencies in the slow-exchange region of the two coalescing resonances. Slow exchange was assumed at 20 °C; i.e., $\nu_A{}^0$ and $\nu_B{}^0$ were assigned to peak positions in the ^{1}H NMR spectrum of (Cl--PPh) at 20 °C. The data obtained, given in Table V, were used to construct a plot of ln (k/T) vs. $1/T$ (Figure 6).

X-ray Crystallography. An asymmetric unit contained three molecules of benzene and included 101 non-hydrogen atoms: $[Pt_2ClP_5C_{68}H_{59}](PF_6)$, corresponding to a formula weight of 1836.08. The unit cell was found to have the following cell parameters: a = 21.604 (6) Å, b = 23.810 (3) Å, c = 15.304 (3) Å, β = 92.14 (4)°, V = 7866 (3) Å^3, Z = 4, ρ_{calcd} = 1.550 g/cm^3, μ = 39.54 cm^{-1}. Single crystals of solvated $[Pt_2(\mu\text{-dppm})_2Cl(PPh_3)](PF_6)$ were formed by slow evaporation of benzene/CH_2Cl_2 solutions at 10 °C. These small crystals were then digested in a stoppered vial at ambient temperature over a period of weeks until single crystals of a suitable size were formed. A yellow crystal (approximate dimensions 1.0 × 0.1 × 0.2 mm) was wedged into a Lindeman glass capillary containing a small amount of mother liquor to prevent loss of solvent and fracturing of the crystal, after which the capillary was sealed.

The capillary was then aligned on a Syntex $P2_1$ diffractometer (graphite-monochromated Mo Kα radiation, λ = 0.71069 Å). All diffraction data were collected at −20 °C. The approximate positions of 15 reflections selected from the rotation picture were used as input into an automatic indexing program.[27] The resulting reduced cell and reduced-cell scalars indicated a monoclinic crystal system, which was confirmed by the symmetry in the axial ω-oscillation photograph for each axis.

Accurate unit cell parameters were obtained by a least-squares fit to tuned 2θ values of 13 reflections ($20 < 2\theta < 35°$).

All data (10987 reflections) within a sphere of $2\theta \leq 45°$ in hkl and $hk\bar{l}$ octants were measured by using an ω-step scan procedure with variable scan rates (minimum 4.5°/min, maximum 29.30°/min). As a general check on the electronic and crystal stability, the intensity of reflection $01\bar{8}$ was remeasured every 75 reflections. This standard reflection was not observed to vary significantly throughout the data collection period. The space group was uniquely identified as $P2_1/n$ by systematic absences occurring when $k = 2n + 1$ for the $0k0$ reflections and $h + l = 2n + 1$ for the $h0l$ reflections. The intensity data were corrected for the Lorentz, polarization, and absorption effects but not for the extinction. Symmetry-related reflections were averaged together, yielding 5611 independent observed ($I \geq 2\sigma_I$ and $F \geq 4\sigma_F$) reflections. The internal consistency factor ($R_I = \sum|I - \langle I\rangle|/\sum I$) was 0.057.

Table VI. Positional and Averaged Thermal Parameters for the Non-Phenyl Atoms in $(Cl\text{--}PPh_3)(PF_6)\cdot 3C_6H_6$[a]

atom	x	y	z	U(av)
Pt1	1886.7 (5)	2928.1 (5)	2757.8 (7)	39
Pt2	2605.7 (5)	2988.4 (6)	4208.2 (9)	52
Cl	3174 (7)	3132 (5)	5570 (10)	131
P1	1097 (4)	3044 (3)	1691 (5)	45
P2	1445 (4)	2211 (3)	3497 (5)	40
P3	2625 (4)	3459 (3)	2124 (7)	63
P4	1721 (4)	2946 (5)	4976 (5)	60
P5	3488 (4)	1979 (5)	3447 (10)	97
P6	3478 (6)	1389 (4)	495 (13)	129
F1	3289 (19)	1831 (10)	−176 (25)	174
F2	2875 (13)	1022 (10)	351 (26)	153
F3	3151 (18)	1761 (12)	1180 (26)	190
F4	3708 (15)	946 (12)	1215 (27)	162
F5	4111 (19)	1682 (17)	616 (37)	223
F6	3796 (17)	1027 (11)	−243 (26)	169
C24	1148 (15)	2501 (12)	4554 (17)	47
C35	3318 (16)	3060 (18)	2241 (29)	93

[a] Fractional atomic coordinates are ×10^4; temperature factors (Å^2) are × 10^3; U(av) is the average of U_{11}, U_{22}8, and U_{33}.

Table VII. Selected Intramolecular Distances (Å) for $[Pt_2(\mu\text{-dppm})_2Cl(PPh_3)](PF_6)\cdot 3C_6H_6$

around $Pt_2P_4C_2$ ring		P–C(phenyl)	
atoms	dist	atoms	dist
Pt1–Pt	2.65 (2)	P1–C11A	1.74 (4)
Pt1–P1	2.333 (8)	P1–C11B	1.83 (3)
Pt1–P2	2.276 (7)	P1–C11C	1.90 (5)
Pt1–P3	2.80 (9)	P2–C21A	1.79 (3)
Pt2–P4	2.283 (9)	P2–C21B	1.85 (4)
Pt2–P5	2.271 (12)	P3–C31A	1.81 (4)
Pt2–Cl	2.403 (14)	P3–C31B	1.78 (4)
P2–C24	1.89 (3)	P4–C41A	1.83 (3)
P4–C24	1.74 (3)	P4–C41B	1.69 (5)
P3–C35	1.78 (4)	P5–C51A	1.85 (4)
P5–C35	1.89 (4)	P5–C51B	1.74 (6)
		P5–D51B[a]	1.85 (8)

[a] Second P–C bond distance in the disordered phenyl ring 5B.

The positions of the Pt atoms were obtained from an analysis of a sharpened Patterson map. The positions of the remaining non-hydrogen atoms were determined by successive structure factor and difference electron density map calculations.[28] It was difficult to locate the atomic positions of several carbon atoms in phenyl rings because of large thermal motions and disordering effects. The PF_6 anion was not disordered, but several phenyl rings were disordered including one of the benzene solvent molecules. Ring multipliers for the disordered groups were refined by using isotropic temperature factors for individual atoms and keeping positional parameters fixed. After optimization, these multipliers were fixed and the positional and anisotropic thermal parameters for Pt, Cl, P, F, and methylene carbons and the isotropic thermal parameters for the rest of the atoms were refined by a block-matrix least-squares procedure minimizing the function $\sum w(|F_o| - |F_c|)^2$, where $w = 1/\sigma_F{}^2$. Examination of $\langle w|F_o| - |F_c|^2\rangle$ with respect to $|F_o|$ and $(\sin\theta)/\lambda$ showed

(27) Jacobson, R. A. *J. Appl. Crystallogr.* **1976**, *9*, 115.

(28) Calculations were carried out on a VAX 11/780 computer. Structure factor calculations and least-squares refinements were done by using the block-matrix/full-matrix programs ALLS (Lapp, R. L.; Jacobson, R. A. U.S. Department of Energy Report IS-4708; Iowa State University: Ames, IA, 1979), Fourier series calculations were done by using the program FOUR (Powell, D. R.; Jacobson, R. A. U.S. Department of Energy Report IS-4737; Iowa State University: Ames, IA, 1980), and for molecular drawing the program ORTEP (Johnson, C. K. U.S. Atomic Energy Commission Report ORNL-3794; Oak Ridge National Laboratory: Oak Ridge, TN, 1970) was used. An empirical absorption correction was carried out by using diffractometer ϕ-scan data and the program ASBN (Karcher, B. A. Ph.D. Dissertation, Iowa State University, 1981).

overweighting at large $|F_o|$ and small $(\sin\theta)/\lambda$. Weights were subsequently adjusted to reduce the variation in $\langle w|F_o| - |F_c|)^2\rangle$ as a function of these variables.

The hydrogen positions were calculated by assuming ideal geometries with the C–H bond distance set to 1.0 Å. The least-squares procedure converged to a conventional residual index of $R = \sum||F_o| - |F_c||/\sum|F_o| = 0.108$ and a weighted residual index of $R_w = [\sum w(|F_o| - |F_c|)^2/\sum w|F_c|^2]^{1/2} = 0.110$. The atomic scattering factors were those from ref 29.

The final positional and thermal parameters are listed in Table VI for atoms in the $Pt_2(\mu\text{-dppm})_2$ ring, while bond angles and lengths for atoms other than phenyl carbons are listed in Tables I and VII, respectively. The final positional and thermal parameters for phenyl carbons and hydrogen atoms and anisotropic thermal parameters as well as bond distances and angles of carbons within the phenyl rings are found in the supplementary material accompanied by least-squares planes of these rings, selected torsional angles for atoms in the $Pt_2(\mu\text{-dppm})_2$ ring, and an ORTEP drawing of the disordered phenyl groups.

Acknowledgment. This work, based in part on the Ph.D. thesis of R.J.B., was supported by the U.S. Department of Energy, Office of Basic Energy Sciences, Division of Chemical Sciences, under Contract W-7405-Eng-82. We are grateful to Professors J. G. Verkade and W. S. Trahanovsky for useful discussions. The Nicolet NT-300 NMR spectrometer was purchased in part with funds from a grant (No. CHE-3209709) from the National Science Foundation to the Department of Chemistry at Iowa State University.

Registry No. $(Cl\text{--}PPh_3)(PF_6)\cdot 3C_6H_6$, 100230-50-0; (Cl--Cl), 61250-65-5; $(I\text{--}PPh_3)^+$, 100230-51-1; (I--I), 61289-07-4; $(Ph_3P\text{--}PPh_3)^{2+}$, 69215-88-9; $(Cl\text{--}dppm)^+$, 100230-52-2.

Supplementary Material Available: Tables reporting full structural parameters and an ORTEP drawing of the disordered phenyl groups (21 pages). Ordering information is given on any current masthead page.

(29) "International Tables for X-ray Crystallography"; Kynoch Press: Birmingham, England, 1974; Vol. IV, pp 71–79. "International Tables for X-ray Crystallography"; Kynoch Press: Birmingham, England, 1962; Vol. IV, pp 215–216.

Contribution from the Department of Chemistry and Laboratory for Molecular Structure and Bonding, Texas A&M University, College Station, Texas 77843

Tetramethyldiplatinum(III) (Pt–Pt) Complexes with 2-Hydroxypyridinato Bridging Ligands

Daniel P. Bancroft, F. Albert Cotton,* Larry R. Falvello, and Willi Schwotzer

Received September 24, 1985

Four compounds of the type $[Pt_2(CH_3)_4(\mu\text{-xhp})_2L_n]$, in which xhp^- is one of the anions 2-oxypyridine (hp^-), 2-oxy-6-fluoropyridine (fhp^-), 2-oxy-6-chloropyridine (chp^-), or 2-oxy-6-methylpyridine (mhp^-), have been prepared and characterized. The general preparative method is to react $[Pt(CH_3)_2(\mu\text{-}C_2H_5)_2S]_2$ (**1**) with the appropriate silver salt. The compound $[Pt_2(CH_3)_4(O_2CCH_3)_2(py)_2]$ (**2**) has also been prepared and structurally characterized, and the crystal structure of the starting material, **1**, has been determined. For **1**, a centrosymmetric structure, in which $(C_2H_5)_2S$ ligands bridge $Pt(CH_3)_2$ units to give a planar four-membered ring with ∠Pt–S–Pt = 100.1 (1)° and ∠S–Pt–S = 79.9 (1)°, is found. The crystals are triclinic ($P\bar{1}$), with a = 7.481 (5) Å, b = 9.114 (3) Å, c = 9.163 (5) Å, α = 90.60 (4)°, β = 113.62 (4)°, γ = 93.41 (4)°, V = 571.0 (5) Å^3, and Z = 1. For compound **2**, which forms orthorhombic crystals (*Ibca*) with a = 16.007 (6) Å, b = 17.443 (4) Å, c = 15.051 (5) Å, V = 4202 (2) Å^3, and Z = 8, a Pt–Pt distance of 2.529 (1) Å is found. Compound **3**, $[Pt_2(CH_3)_4(hp)_2(py)_2]\cdot 2CHCl_3$, forms orthorhombic crystals ($P2_12_12_1$), with a = 14.174 (4) Å, b = 24.485 (8) Å, c = 9.820 (2) Å, V = 3408 (2) Å^3, and Z = 4, and has a Pt–Pt distance of 2.550 (1) Å. Compound **4**, $[Pt_2(CH_3)_4(fhp)_2(py)_2]\cdot 0.17C_6H_6$, forms trigonal crystals ($R\bar{3}$), with $a = b$ = 32.767 [17] Å, c = 12.629 (2) Å, V = 11 743 (14) Å^3, and Z = 18, and has a Pt–Pt distance of 2.551 (2) Å. Compound **5**, $[Pt_2(CH_3)_4(chp)_2(py)]$, which forms triclinic crystals ($P\bar{1}$) with a = 8.839 (4) Å, b = 9.475 (4) Å, c = 13.109 (6) Å, α = 92.00 (3)°, β = 90.61 (4)°, γ = 96.38 (4)°, V = 1090 (2) Å^3, and Z = 2, has a Pt–Pt distance of 2.545 (1) Å. Lastly, compound **6**, $[Pt_2(CH_3)_4(mhp)_2(py)]$, forms triclinic crystals ($P\bar{1}$), with a = 8.005 (1) Å, b = 8.774 (2) Å, c = 15.970 (3) Å, α = 94.16 (2)°, β = 90.27 (2)°, γ = 100.63 (1)°, V = 1099.2 (7) Å^3, and Z = 2, and has a Pt–Pt distance of 2.543 (1) Å. In complexes **3–6**, the geometry is dependent upon the size of the substituent on the pyridine ring. If the substituent is relatively small (i.e., H or F), the complex contains a nonpolar arrangement of bridging ligands and both axial positions are occupied. When the substituent is large (i.e., Cl or CH_3), a polar arrangement of the bridging ligands is observed and one of the axial sites is vacant due to steric interference from the ligand substituent. This results in complexes in which one platinum atom is formally 5-coordinate and the other platinum atom is formally 6-coordinate.

Introduction

Although the earliest reports of diplatinum(III) chemistry appeared in the first decade of this century,[1] it has only been within the last 12 years that a systematic development of such chemistry has taken place.[2,3] One class of these compounds are those of the type $[Pt_2R_4(O_2CR')_2L_2]$, where R = Ph and Me, R′ = one of a variety of organic radicals, and L = one of a variety of donors. These were first prepared and described in 1976 and 1977 by Vrieze and co-workers,[4,5] who synthesized them from the $[PtR_2(\mu\text{-}Et_2S)]_2$ starting materials[6,7] by the following type of reaction sequence:

$$[Pt_2(CH_3)_4(R_2S)_2] + 2Ag(O_2CR') \rightarrow [Pt_2(CH_3)_4(O_2CR')_2(R_2S)_2] + 2Ag^0$$

$$[Pt_2(CH_3)_4(O_2CR')_2(R_2S)_2] + \text{excess pyridine} \rightarrow [Pt_2(CH_3)_4(O_2CR')_2(py)_2] + 2R_2S$$

Only one of these compounds, $[Pt_2(CH_3)_4(O_2CCF_3)_2(4\text{-}MeC_5H_4N)_2]$, has been structurally characterized by X-ray crystallography.[8]

(1) (a) Blondel, M. *Ann. Chim. Phys.* **1905**, *8*, 110. (b) Wohler, L.; Frey, W. *Z. Elektrochem.* **1909**, *15*, 132. (c) Delephine, M. *C. R. Hebd. Seances Acad. Sci.* **1910**, *150*, 104.
(2) O'Halloran, T. V.; Lippard, S. J. *Isr. J. Chem.* **1985**, *25*, 130.
(3) Cotton, F. A.; Walton, R. A. *Struct. Bonding*, in press.
(4) Kuyper, J.; Vrieze, K. *Transition Met. Chem.* (*Weinheim, Ger.*) **1976**, *1*, 208.
(5) Steele, B. R.; Vrieze, K. *Transition Met. Chem.* (*Weinheim, Ger.*) **1977**, *2*, 169.
(6) Kuyper, J.; van der Laan, R.; Jeanneaus, F.; Vrieze, K. *Transition Met. Chem.* (*Weinheim, Ger.*) **1976**, *1*, 199.
(7) Steele, B. R.; Vrieze, K. *Transition Met. Chem.* (*Weinheim, Ger.*) **1977**, *2*, 140.

0020-1669/86/1325-0763$01.50/0